

One-dimensional quantum antiferromagnetism in the p -orbital CsO_2 compound revealed by electron paramagnetic resonance

Tilen Knaflič,¹ Martin Klanjšek,² Annette Sans,³ Peter Adler,³
Martin Jansen,^{3,4} Claudia Felser,³ and Denis Arčon^{2,5,*}

¹*Jožef Stefan Institute, Jamova 39, SI-1000 Ljubljana, Slovenia*

²*Jožef Stefan Institute, Jamova 39, SI-1000 Ljubljana, Slovenia*

³*Max-Planck-Institut für Chemische Physik fester Stoffe, 01187 Dresden, Germany*

⁴*Max-Planck-Institut für Festkörperforschung, 70569 Stuttgart, Germany*

⁵*Faculty of Mathematics and Physics, University of Ljubljana, Jadranska 19, SI-1000 Ljubljana, Slovenia*

Recently it was proposed that the orbital ordering of $\pi_{x,y}^*$ molecular orbitals in the superoxide CsO_2 compound leads to the formation of spin-1/2 chains below the structural phase transition occurring at $T_{s1} = 61$ K on cooling. Here we report a detailed X-band electron paramagnetic resonance (EPR) study of this phase in CsO_2 powder. The EPR signal appears as a broad line below T_{s1} , which is replaced by the antiferromagnetic resonance below the Néel temperature $T_N = 8.3$ K. The temperature dependence of the EPR linewidth between T_{s1} and T_N agrees with the predictions for the one-dimensional Heisenberg antiferromagnetic chain of $S = 1/2$ spins in the presence of symmetric anisotropic exchange interaction. Complementary analysis of the EPR lineshape, linewidth and the signal intensity within the Tomonaga-Luttinger liquid (TLL) framework allows for a determination of the TLL exponent $K = 0.48$. Present EPR data thus fully comply with the quantum antiferromagnetic state of spin-1/2 chains in the orbitally ordered phase of CsO_2 , which is, therefore, a unique p -orbital system where such a state could be studied.

PACS numbers: 75.10.Pq, 71.10.Pm, 76.30.-v

I. INTRODUCTION

Quantum antiferromagnets have provided one of the most fertile grounds for discoveries of new states of matter and testing the theoretical models. The one-dimensional Heisenberg antiferromagnetic chain of $S = 1/2$ spins (1D-HAF) is probably the most studied example of such quantum antiferromagnets where recent advances in the theoretical approaches^{1–4} have enabled quantitative discussion of experimental data on model systems. Among the best realizations of 1D-HAFs are KCuF_3 ,^{5–8} Sr_2CuO_3 ,^{9–11} $\text{CuSO}_4 \cdot 5\text{D}_2\text{O}$,¹² $\text{Cu}(\text{C}_4\text{H}_4\text{N}_2)(\text{NO}_3)_2$,^{13–15} copper-pyrimidine-dinitrate¹⁶ and CuSe_2O_5 .^{17–19} Excellent agreement between the extensive experimental and theoretical work established the existence of gapless $S = 1/2$ excitations, the so called spinons,²⁰ into which the conventional $S = 1$ magnon excitations fractionalize. The low-energy description of gapless phases in 1D-HAFs leads to the Tomonaga-Luttinger liquid (TLL) paradigm¹ as a universal concept of quantum physics in one dimension, beyond the perturbation theory.

In all the above-cited realizations of 1D-HAFs, the spin states stem from the electrons in d -orbitals of transition metal ions. Recently, an important structural and magnetic susceptibility investigation of CsO_2 , a member of the alkali superoxide AO_2 (A = alkali metal) family,^{21–30} suggested this compound to realize the first p -orbital 1D-HAF.²⁷ 1D-HAF state is established in the orbitally-ordered phase below $T_{s1} = 61$ K on cooling, where a spatial alignment of the $\pi_{x,y}^*$ molecular orbitals of O_2^- units with $S = 1/2$ results in a strong superexchange interaction J along the crystallographic b -axis, i.e., the

chain axis, while in the perpendicular crystallographic a -direction the exchange interaction is very small due to poor overlap of the corresponding molecular orbitals (Fig. 1). Comprehensive ^{133}Cs nuclear magnetic resonance (NMR) measurements of spin-lattice relaxation rate T_1^{-1} in different magnetic fields indeed revealed the characteristic power law dependence $T_1^{-1} \propto T^\nu$,²⁹ which is a hallmark of the TLL state.^{31,32} The field-dependence of the extracted parameters quantitatively demonstrates that the low-energy spectrum of spin-fluctuations in the 1D-HAF state of CsO_2 can be described in terms of TLL yielding a dimensionless TLL exponent $K \approx 1/4$, consistent with the Ising-like exchange-coupling anisotropy. Because the proposed 1D-HAF state in CsO_2 is based on p -orbital states that occupy a different regime of interplay between magnetism, structure, vibrations, and orbital ordering than the more conventional d -orbital or f -orbital states, finding additional independent experimental evidences for the 1D-HAF state is highly desirable.

Electron paramagnetic resonance (EPR) is a resonance technique that has been broadly used to study low-dimensional quantum antiferromagnets.³³ Traditionally, temperature dependence of the shift and linewidth of the EPR spectra have been discussed with the spectral moment analysis, i.e., the so-called Kubo-Tomita theory.³⁴ However, this approach was suggested to be inappropriate in the case of 1D-HAFs. Instead, Oshikawa and Affleck employed the sine-Gordon quantum-field theory to circumvent some computational difficulties of the quantum spin state in 1D-HAFs and to predict the temperature dependence of the EPR linewidth for different magnetic anisotropies.^{2,3} Experimental tests on model sys-

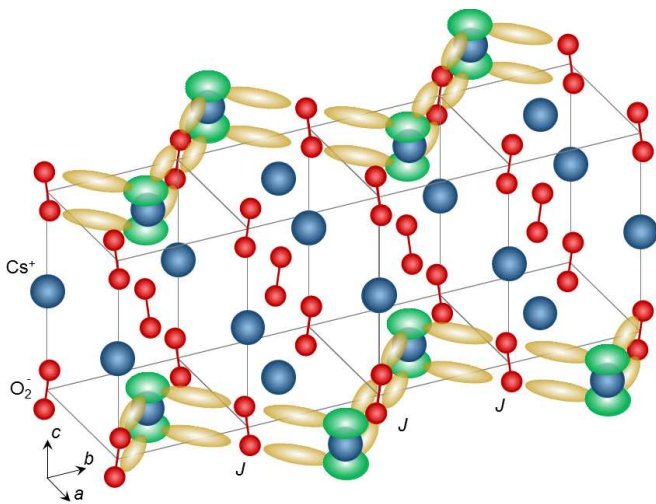


FIG. 1. (color online) Sketch of the CsO_2 crystal structure and relevant orbitals. Zig-zag chains of ordered $\text{O}_2^- \pi_{x,y}^*$ molecular orbitals ($S = 1/2$) run along the crystallographic b -axis. Blue and red spheres represent caesium and oxygen atoms, respectively. The superexchange interactions, J , between $\pi_{x,y}^*$ orbitals (yellow) are bridged by Cs p_z orbitals (green).

tems showed an excellent agreement with this theory.^{16,18} Interestingly, exact low-energy solutions for EPR spectra in terms of TLL exist in the spin channel only for metallic wires³⁵ and are still missing for the case of insulating spin-chain systems. First EPR studies of CsO_2 single crystals were reported already back in the 1970's by Känzig,³⁰ but clearly the experimental data need to be reinterpreted in light of the new findings. Therefore, we decided to remeasure the X-band EPR spectra and to test the data against the Oshikawa-Affleck and the TLL theories. An excellent agreement is found with both theoretical models below T_{s1} , thus providing an independent support for the 1D-HAF state in CsO_2 . Therefore, CsO_2 indeed represents a rare example of the p -orbital one-dimensional quantum antiferromagnet.

II. EXPERIMENTAL METHODS

The CsO_2 powder sample came from the same batch as the one used in our previous NMR study where the preparation was described in detail.²⁹ Freshly distilled Cs metal was oxidized with $^{17}\text{O}_2$ gas. To homogenize the yellow product of Cs^{17}O_2 , several cycles of grinding under a controlled argon atmosphere and temperature annealing in natural O_2 was processed. The sample was enriched by the ^{17}O isotope to approximately 50%, according to Raman spectroscopy. Laboratory X-ray diffraction at room temperature confirmed high purity of the sample, as all peaks could be indexed to the tetragonal, $I4/mmm$, structure of CsO_2 . No impurity phase could be traced down to the resolution of our XRD equipment.

The magnetic properties of the sample, which were first

checked by SQUID magnetometry,²⁹ are in good agreement with previous results.²⁷ In particular, an inflection in the magnetic susceptibility curve $\chi(T)$ occurring near 70 K on heating ascribed to the structural/orbital ordering transition and a broad hump near 30 K implying the 1D-HAF state, are clearly visible. A Curie-Weiss analysis of the high-temperature $\chi^{-1}(T)$ data obtained in a field of 0.5 T yields an effective magnetic moment μ_{eff} of $2.01\mu_B$ (here, μ_B is Bohr magneton) and a Curie-Weiss constant $\theta_{\text{CW}} = -7$ K. Similarly as in Ref. 27, μ_{eff} is considerably larger than the spin-only value of $\mu_{\text{eff}} = 1.73\mu_B$ for an $S = 1/2$ system, thus confirming an orbital contribution to μ_{eff} in the high temperature phase of CsO_2 . The Néel ordering transition below 10 K is mostly obscured by a low-temperature Curie tail due to a small amount of paramagnetic impurities. However, a weak feature in $\chi(T)$ around 9 K in data measured at low magnetic field of 0.01 T indicates the transition to the ordered state.

For the EPR measurements, 23.1 mg of powder sample was sealed under dynamic vacuum in a standard Suprasil quartz tube. The X-band EPR experiments were performed on a home-built spectrometer equipped with a Varian E-101 microwave bridge, a Varian TEM104 dual cavity resonator, an Oxford Instruments ESR900 cryostat and an Oxford Instruments ITC503 temperature controller. The temperature stability was better than ± 0.05 K at all temperatures. The EPR spectra were measured on cooling.

III. RESULTS AND DISCUSSION

Temperature evolution of the X-band EPR spectra. The CsO_2 powder sample shows no detectable X-band EPR signal at room temperature. On cooling, a very broad line starts to appear below ~ 70 K and becomes very pronounced below T_{s1} (Fig. 2). For temperatures close to T_{s1} , the EPR spectrum is shifted towards higher fields relative to $g \approx 2$, thus indicating an orbital angular momentum contribution in the high-temperature orbitally-disordered phase and consistent with the large high-temperature μ_{eff} extracted from the SQUID data.^{27,29} However, as temperature decreases well below T_{s1} , the EPR signal narrows and shifts to $g \approx 2$ resonance-field range. The powder spectra are well fitted with the uniaxial g -factor anisotropy, i.e., $g_{xx} = g_{yy} \neq g_{zz}$, convoluted with a Lorentzian lineshape broadening whose linewidth also has the uniaxial anisotropy, i.e., $\Delta B_x = \Delta B_y \neq \Delta B_z$. At $T = 15$ K, an unconstrained fit converges to $g_{xx} = g_{yy} = 1.8886$ and $g_{zz} = 2.6963$, which agree with the literature data obtained on single crystals.³⁰ Moreover, since we consistently find $\Delta B_x \approx \Delta B_z/2$ at all temperatures, we next constrain $2\Delta B_x = \Delta B_z \equiv \Delta B$ to find that ΔB nearly linearly decreases with decreasing temperature between 60 and ~ 20 K. The EPR spectrum is the narrowest at $T = 15$ K where $\Delta B = 249$ mT. On further cooling, the signal broadens again as the Néel

temperature $T_N = 8.3$ K is approached from above before it completely disappears below T_N and is replaced by another slightly asymmetric signal shifted to significantly lower fields. For example, at $T = 7$ K this new resonance is centered at around 80 mT. Since this signal is found only below T_N , we tentatively assign it to one of the antiferromagnetic resonance modes. At lowest temperatures we notice another extremely weak peak at $g \approx 2.06$, which we attribute either to impurity O_2^- centers or to point defects in the antiferromagnetically ordered magnetic lattice.

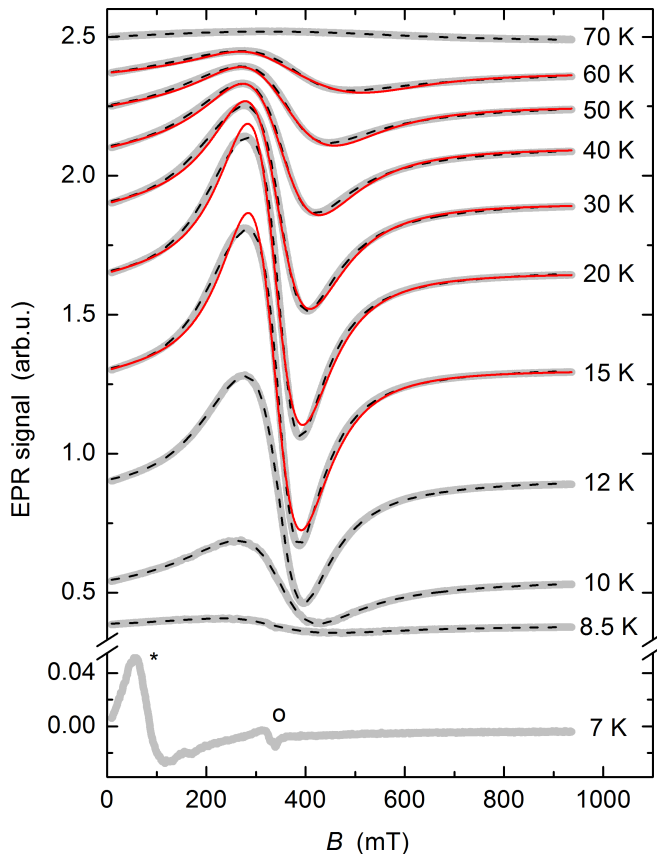


FIG. 2. (color online) The temperature evolution of the X-band EPR spectra in CsO_2 powder (grey lines). Dashed black lines are fits with the uniaxial g -factor and linewidth anisotropy ($g_{xx} = g_{yy} \neq g_{zz}$ and $\Delta B_x = \Delta B_y = \Delta B_z/2$). Solid red lines are fits with Eq. (3) to the TLL spectrum. Below the Néel temperature $T_N = 8.3$ K the paramagnetic EPR signal completely disappears and antiferromagnetic resonance (marked by *) is observed at around 80 mT at 7 K. At 7 K we observe also an extremely weak impurity line at $g \approx 2.06$ (marked by o).

Linewidth analysis with the Oshikawa-Affleck theory. As recent structural and NMR investigations of CsO_2 interpreted the phase that develops below T_{s1} as a 1D-HAF phase,^{27,29} we proceed to discuss the measured EPR spectra (Fig. 2) in terms of the one-dimensional magnetism. We start with the Oshikawa-Affleck theoretical framework of a low-temperature EPR response in $S = 1/2$

one-dimensional Heisenberg antiferromagnets, which predicts distinct temperature dependences of EPR linewidth for the case of anisotropic exchange broadening, where $\Delta B \propto T$, as opposed to the case of staggered-field broadening, where $\Delta B \propto (B/T)^2$.³ Since we find that ΔB nearly linearly increases with increasing temperature between 15 K and T_{s1} (Fig. 3a), we conclude that the main anisotropic interaction that broadens EPR spectra is the symmetric anisotropic exchange interaction. A rapid increase in ΔB on cooling between 15 K and T_N is attributed to the critical fluctuations just before the three-dimensional antiferromagnetic order sets in. In the temperature range between T_{s1} and T_N , the temperature dependence of ΔB is thus fitted to

$$\Delta B = \frac{2\epsilon k_B \delta^2}{g\mu_B \pi^3} T + \Delta B_{cf} \left(\frac{T - T_N}{T_N} \right)^{-\alpha}, \quad (1)$$

which comprises linewidth contributions from the 1D-HAF phase with symmetric anisotropic exchange³ and from the critical fluctuations, respectively. Here, k_B is the Boltzmann constant. The constant ϵ amounts to 2 for magnetic field directed along the anisotropy axis and to 1 for the perpendicular case, thus nicely accounting for the experimental observation $\Delta B_x = \Delta B_z/2$. Since we have defined $\Delta B = \Delta B_z$, we use $\epsilon = 2$ in Eq. (1). An excellent fit of the experimental EPR linewidth (Fig. 3a) yields the constant of symmetric anisotropic exchange $\delta = 0.35J$. Although we cannot determine the sign of δ , because the corresponding linewidth term is proportional to δ^2 , we note a significant magnetic anisotropy that is consistent with the NMR finding of the Ising-like exchange-coupling anisotropy. The magnitude of the critical fluctuations is found to be $\Delta B_{cf} = 0.12$ T and the critical exponent $\alpha = 0.6$.

Analysis of the EPR spectra within the Tomonaga-Luttinger-Liquid framework. The above analysis demonstrates that the EPR data of CsO_2 may indeed be interpreted with the 1D-HAF model, at least for $15 \text{ K} < T < T_{s1}$. However, a recent ^{133}Cs NMR study of CsO_2 employed the TLL formalism instead,²⁹ so that it is difficult to directly compare the two results. Therefore, for the quantitative comparison with the NMR data we next test our EPR data also against the TLL model.

The EPR spectrum $I(\omega, B)$ is given by the imaginary part of the dynamical spin susceptibility for the transverse direction (i.e., perpendicular to the magnetic field), $\chi''_{\perp}(q, \omega, B)$, calculated at the momentum of the excitation $q = 0$ and at the resonant frequency ω , namely $I(\omega, B) = \frac{B_{\perp}^2}{2\mu_0} \omega \chi''_{\perp}(q = 0, \omega, B) V$.³⁶ Here, B_{\perp} is the magnitude of the perpendicular (excitation) microwave field, μ_0 the permeability of the vacuum and V the volume of the sample. We stress at this point that the EPR spectrum provides complementary information to the NMR spin-lattice relaxation rate, which is proportional to $\chi''_{\perp}(q, \omega, B)$ integrated over the Brillouin zone. At low frequencies, the dynamical spin susceptibility has nonzero contributions in the vicinity of the four Q vectors

in the Brillouin zone, i.e., π and $2\pi m$ for the transverse direction, and 0 and $\pi(1 - 2m)$ for the longitudinal direction (i.e., along the magnetic field). Here m is the field-induced magnetization, which is related to the two TLL parameters, i.e., the dimensionless exponent K and the velocity of spin excitations u , via $m = BK/\pi u$. The first and the third of the listed modes are commensurate, whereas the other two modes are field-dependent (through m) and thus incommensurate. Among these, the EPR spectrum is determined by the transverse mode with nonzero contribution close to $q = 0$, i.e., by the mode at $Q = 2\pi m$. For this mode the dynamical spin susceptibility takes the form¹

$$\chi''_{\perp}(q, \omega, T) = -C'_3 T^{2\gamma} \left[\beta\left(\frac{\gamma+2}{2} - \frac{i(\omega + u\delta q)}{4\pi T}, (-1 - \gamma)\right) \beta\left(\frac{\gamma}{2} - \frac{i(\omega - u\delta q)}{4\pi T}, (1 - \gamma)\right) + \beta\left(\frac{\gamma}{2} - \frac{i(\omega + u\delta q)}{4\pi T}, (1 - \gamma)\right) \beta\left(\frac{\gamma+2}{2} - \frac{i(\omega - u\delta q)}{4\pi T}, (-1 - \gamma)\right) \right], \quad (2)$$

where $q = Q + \delta q$ and δq is small. Here, C'_3 is the non-universal amplitude,¹ β is the Euler's beta function and $2\gamma = 2K + 1/(2K) - 2$. To satisfy the EPR resonance condition $q = 0$, we have to set $\delta q = -Q$, which finally leads to

$$I(\omega, B, T) = -I_0 \omega T^{2\gamma} \text{Im}[F(2 + \gamma, k_1)F(\gamma, k_2) + F(2 + \gamma, k_2)F(\gamma, k_1)]. \quad (3)$$

The signal-intensity prefactor I_0 is proportional to the electronic static spin susceptibility χ_0 , to B_{\perp} and V . The arguments $k_{1,2} = (\hbar\omega \mp 2g\mu_B KB)/(2\pi k_B T)$ and the function $F(x, y) = \beta[(x - iy)/2, 1 - x]$. We stress that Eq. (3) is analogous to the one calculated for the spin channel of the correlated one-dimensional metals, e.g., carbon nanotubes.³⁵ Fitting all the experimental X-band EPR spectra (Fig. 2) in the temperature range $15 \text{ K} \leq T \leq 60 \text{ K}$ to $dI(\omega, B, T)/dB$ with I_0 and K as the only free parameters produces excellent lineshape fits (solid red lines in Fig. 2) yielding $K = 0.48$. We note that large broadening of the EPR spectra is found as soon as K deviates significantly from $1/2$, which is again reminiscent of the case of interacting itinerant electrons in one dimension.³⁵

The temperature dependence of the EPR signal intensity is shown in Fig. 3b. The intensity shows a broad maximum at $T_{\text{max}} \approx 22 \text{ K}$ and is rapidly suppressed upon approaching the Néel temperature from above. We note that T_{max} matches the temperatures of the maxima in the bulk susceptibility measurements²⁷ and in the local spin susceptibility probed by ^{133}Cs NMR.²⁹ The best fit of the EPR signal intensity to the 1D-HAF spin susceptibility³⁷ in the temperature range from 60 K to 15 K is found for $J = 35 \text{ K}$, which is close to the corresponding $J = 40 \text{ K}$ extracted from the magnetic susceptibility²⁷ and ^{133}Cs

NMR data.²⁹ The deviations of the fit from the data points close to T_{s1} are expected due to a large lineshape broadening and lineshift in this temperature range (Fig. 2), implying underestimated data values, whereas the discrepancies below $\sim 15 \text{ K}$ are due to the onset of three-dimensional antiferromagnetic correlations. The temperature dependence of the EPR signal intensity and the magnitude of the extracted J thus fully corroborate the proposed TLL state below T_{s1} .

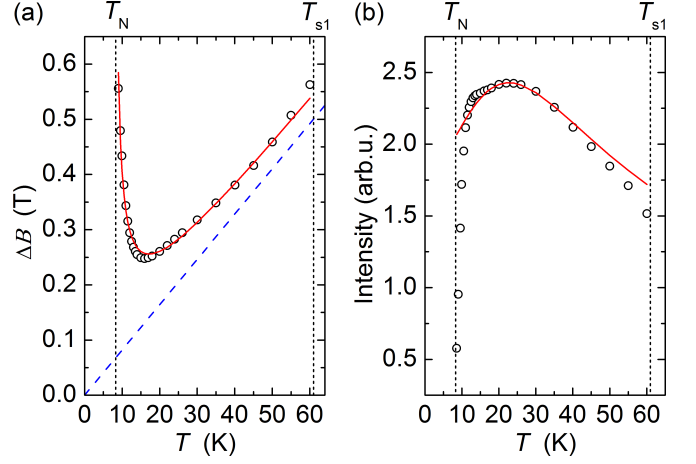


FIG. 3. (color online) (a) Temperature dependence of the X-band EPR linewidth as obtained from the lineshape fits of CsO_2 spectra (open black circles). Solid red line represents fits to Eqs. (1) or (5), which are undistinguishable. Dashed blue line shows the contribution of the 1D-HAF phase to the total EPR linewidth. (b) Temperature dependence of the X-band EPR signal intensity of CsO_2 (open black circles). Solid red line is fit to the static spin susceptibility of the 1D-HAF³⁷ with $J = 35 \text{ K}$. Dotted vertical black lines mark the Néel ($T_N = 8.3 \text{ K}$) and orbital-ordering temperatures ($T_{s1} = 61 \text{ K}$).

Finally, since in our case $\gamma \ll 1$ and $k_B T \gg \hbar\omega, g\mu_B B$, we can by using arguments of Ref. 35 simplify Eq. (3) to a sum of two Lorentzian components, one centered at the positive and the other one at the negative resonance field, with the temperature-dependent linewidth

$$\Delta B_{\text{TLL}} = \frac{4\pi\gamma k_B}{g\mu_B} T. \quad (4)$$

Not surprisingly, in this limit the temperature dependence of the EPR linewidth takes, in terms of the temperature dependence, the same form as Eq. (1). Therefore, fitting the experimental linewidth to

$$\Delta B = \Delta B_{\text{TLL}} + \Delta B_{\text{cf}} \left(\frac{T - T_N}{T_N} \right)^{-\alpha}, \quad (5)$$

and using the same parameters for critical fluctuations ΔB_{cf} and α as above, we find $K = 0.48$ consistent with the value of K obtained from the EPR lineshape fits. To solve the problem of antiferromagnetically coupled $S = 1/2$ spins in one dimension, both the Oshikawa-Affleck and the TLL theories bosonize the spin operators and

then use field-theory approaches. However, to calculate the EPR response, the older Oshikawa-Affleck theory^{2,3} calculates the EPR width and shift perturbatively. The exact solutions for the dynamic spin susceptibilities were published only later¹ and here we take a full advantage of these newly made discoveries to calculate exactly the EPR spectrum. Given the same starting point for the Oshikawa-Affleck and the TLL approaches, it is thus not surprising that both theories equally well describe the EPR spectra in the parameter range relevant for CsO₂.

The most important finding of this work is thus that the temperature dependence of the EPR lineshape, the EPR linewidth, and the EPR signal intensity fully comply with the interpretation of the orbitally-ordered phase of CsO₂ in terms of TLL framework, with K consistently converging to the value close to but yet slightly smaller than $1/2$. The extracted K and the symmetric anisotropy-exchange δ places CsO₂ on the Ising-anisotropy side of the phase diagram. Although this conclusion in general agrees with the previous analysis of the ¹³³Cs NMR data²⁹, we note that $K \approx 1/2$ derived from the present EPR data is notably larger than $K \approx 1/4$ extracted from the high-field ($2.35 < B < 9.4$ T) NMR experiments on the same sample. This discrepancy remains puzzling. However, since EPR and NMR probe the low-energy part of $\chi''_{\perp}(q, \omega)$ in a slightly different way, the features in the excitation spectrum arising from the effects of interchain couplings may echo differently in EPR and NMR data. The origin of the symmetric anisotropic exchange is unclear at the moment, but most likely it directly reflects the fact that the Cs⁺ ions, characterized by a significant spin-orbit coupling constant, are bridg-

ing the superexchange between nearest neighboring O₂⁻ units along the b -axis.

IV. CONCLUSIONS

In conclusion, a systematic analysis of the X-band EPR spectra in the low-temperature orbitally-ordered phase of CsO₂ agrees with the proposed 1D-HAF state. Using either the Oshikawa-Affleck or the TLL theoretical frameworks, we find a systematic agreement with the experimental EPR lineshape, linewidth and signal intensity, thus allowing us a quantitative determination of the anisotropy of the symmetric exchange interaction or, alternatively, of the TLL exponent. Therefore, our results indeed comply with CsO₂ as a p -orbital system showing a quantum antiferromagnetic state where orbital ordering is pivotal in the formation of $S = 1/2$ spin chains. Since similar orbital-ordering physics is ubiquitous to the whole family of AO₂ superoxide compounds^{21–29} and A₄O₆^{38,39} sesquioxide compounds, it would be interesting to test in the future the low-dimensional quantum magnetism also in these systems.

ACKNOWLEDGMENTS

D.A. and C.F. acknowledge the financial support by the European Union FP7-NMP-2011-EU-Japan project LEMSUPER under Contract No. 283214. We thank Walter Schnelle and Ralf Koban for performing magnetization measurements.

* denis.arcon@ijs.si

¹ T. Giamarchi, *Quantum Physics in One Dimension* (Oxford Univ. Press, Oxford, 2004).

² M. Oshikawa and I. Affleck, *Phys. Rev. Lett.* **82**, 5136 (1999).

³ I. Affleck and M. Oshikawa, *Phys. Rev. B* **60**, 1038 (1999); **62**, 9200 (2000).

⁴ K. Schönhammer, *J. Phys.: Condens. Matter* **25**, 014001 (2013).

⁵ B. Lake, D. A. Tennant, C. D. Frost, and S. E. Nagler, *Nature Materials* **4**, 329 (2005).

⁶ B. Lake, D. A. Tennant, J.-S. Caux, T. Barthel, U. Schollwöck, S. E. Nagler, and C. D. Frost, *Phys. Rev. Lett.* **111**, 137205 (2013).

⁷ J. Chakhalian, R.F. Kiefl, R. Miller, S.R. Dunsiger, G. Morris, S. Kreitzman, W.A. MacFarlane, J. Sonier, S. Eggert, I. Affleck, and I. Yamada, *Physica B* **326**, 422 (2003).

⁸ M. V. Eremin, D. V. Zakharov, H.-A. Krug von Nidda, R. M. Eremina, A. Shuvaev, A. Pimenov, P. Ghigna, J. Deisenhofer, and A. Loidl, *Phys. Rev. Lett.* **101**, 147601 (2008).

⁹ N. Motoyama, H. Eisaki, and S. Uchida, *Phys. Rev. Lett.* **76**, 3212 (1996).

¹⁰ M. Takigawa, N. Motoyama, H. Eisaki, and S. Uchida, *Phys. Rev. Lett.* **76**, 4612 (1996).

¹¹ M. Takigawa, O. A. Starykh, A. W. Sandvik, and R. R. P. Singh, *Phys. Rev. B* **56**, 13681 (1997).

¹² M. Mourgil, M. Enderle, A. Klöpperpieper, J.-S. Caux, A. Stunault, and H. M. Rønnow, *Nat. Phys.* **9**, 435 (2013).

¹³ P. R. Hammar, M. B. Stone, Daniel H. Reich, C. Broholm, P. J. Gibson, M. M. Turnbull, C. P. Landee, and M. Oshikawa, *Phys. Rev. B* **59**, 1008 (1999).

¹⁴ T. Lancaster, S. J. Blundell, M. L. Brooks, P. J. Baker, F. L. Pratt, J. L. Manson, C. P. Landee, and C. Baines, *Phys. Rev. B* **73**, 020410(R) (2006).

¹⁵ Y. Kono, T. Sakakibara, C.P. Aoyama, C. Hotta, M.M. Turnbull, C.P. Landee, and Y. Takano, *Phys. Rev. Lett.* **114**, 037202 (2015).

¹⁶ S. A. Zvyagin, A. K. Kolezhuk, J. Krzystek, and R. Feynherm, *Phys. Rev. Lett.* **95**, 017207 (2005).

¹⁷ O. Janson, W. Schnelle, M. Schmidt, Yu Prots, S.-L. Drechsler, S. K. Filatov and H. Rosner, *New J. Phys.* **11**, 113034 (2009).

¹⁸ M. Herak, A. Zorko, D. Arčon, A. Potočnik, M. Klanjšek, J. van Tol, A. Ozarowski, and H. Berger, *Phys. Rev. B* **84**, 184436 (2011).

- ¹⁹ M. Herak, A. Zorko, M. Pregelj, O. Zaharko, G. Posnjak, Z. Jagličić, A. Potočnik, H. Luetkens, J. van Tol, A. Ozarowski, H. Berger, and D. Arčon, *Phys. Rev. B* **87**, 104413 (2013).
- ²⁰ L. D. Faddeev and L. A. Takhtajan, *Phys. Lett. A* **85**, 375 (1981).
- ²¹ W. Hesse, M. Jansen, and W. Schnick, *Prog. Solid State Chem.* **19**, 47 (1989).
- ²² A. K. Nandy, P. Mahadevan, P. Sen, and D. D. Sarma, *Phys. Rev. Lett.* **105**, 056403 (2010).
- ²³ I. V. Solov'yev, *New J. Phys.* **10**, 013035 (2008).
- ²⁴ M. Kim, B. H. Kim, H. C. Choi, and B. I. Min, *Phys. Rev. B* **81**, 100409 (2010).
- ²⁵ I. V. Solov'yev, Z. V. Pchelkina, and V. V. Mazurenko, *CrystEngComm* **16**, 522 (2014).
- ²⁶ K. Wohlfeld, M. Daghofer, and A. M. Oleś, *Europhys. Lett.* **96**, 27001 (2011).
- ²⁷ S. Riyadi, B. Zhang, R. A. de Groot, A. Caretta, P. H. M. van Loosdrecht, T. T. M. Palstra, and G. R. Blake, *Phys. Rev. Lett.* **108**, 217206 (2012).
- ²⁸ S. Riyadi, S. Giriya-pura, R. A. de Groot, A. Caretta, P. H. M. van Loosdrecht, T. T. M. Palstra, and G. R. Blake, *Chem. Mat.* **23**, 1578 (2011).
- ²⁹ M. Klanjšek, D. Arčon, A. Sans, P. Adler, M. Jansen, and C. Felser, arXiv:1409.4818.
- ³⁰ M. Labhart, D. Raoux, W. Känzig, and M. A. Bösch *Phys. Rev. B* **20**, 53 (1979).
- ³¹ M. Jeong, H. Mayaffre, C. Berthier, D. Schmidiger, A. Zheludev, and M. Horvatić, *Phys. Rev. Lett.* **111**, 106404 (2013).
- ³² M. Klanjšek, H. Mayaffre, C. Berthier, M. Horvatic, B. Chiari, O. Piovesana, P. Bouillot, C. Kollath, E. Orignac, R. Citro, and T. Giamarchi, *Phys. Rev. Lett.* **101**, 137207 (2008).
- ³³ Y. Ajiro, *J. Phys. Soc. Jpn.* **72**, 12 (2003).
- ³⁴ A. Bencini, D. Gatteschi, EPR of Exchange Coupled Systems (Springer Verlag, Heidelberg, 1990).
- ³⁵ B. Dóra, M. Gúlcasi, J. Koltai, V. Zólyomi, J. Kürti, and F. Simon, *Phys. Rev. Lett.* **101**, 106408 (2008).
- ³⁶ C. P. Slichter, Principles of Magnetic Resonance (Springer, Berlin, 1978).
- ³⁷ R. Feyerherm, S. Abens, D. Günther, T. Ishida, M. Meißner, M. Meschke, T. Nogami, and M. Steiner, *J. Phys.: Condens. Matter* **12**, 8495 (2000).
- ³⁸ J. Winterlik, G. H. Fecher, C. A. Jenkins, S. Medvedev, C. Felser, J. Kübler, C. Mühle, K. Doll, M. Jansen, T. Palasyuk, I. Trojan, M. I. Erements, and F. Emmerling, *Phys. Rev. B* **79**, 214410 (2009).
- ³⁹ D. Arčon, K. Anderle, M. Klanjšek, A. Sans, C. Mühle, P. Adler, W. Schnelle, M. Jansen, and C. Felser, *Phys. Rev. B* **88**, 224409 (2013).